THE JOURNAL OF BIOLOGICAL CHEMISTRY VOL. 285, NO. 11, pp. 8302–8315, March 12, 2010

Structural and Functional Characterization of a Novel Homodimeric Three-finger Neurotoxin from the Venom of *Ophiophagus hannah* (King Cobra)*[S]◆

Received for publication, October 13, 2009, and in revised form, December 23, 2009 Published, JBC Papers in Press, January 13, 2010, DOI 10.1074/jbc.M109.074161

Amrita Roy[‡], Xingding Zhou[‡], Ming Zhi Chong[‡], Dieter D'hoedt[§], Chun Shin Foo[‡], Nandhakishore Rajagopalan[‡1], Selvanayagam Nirthanan[¶‖], Daniel Bertrand[§], J. Sivaraman[‡], and R. Manjunatha Kini[‡2]**

*From the [‡]Department of Biological Sciences, National University of Singapore, Singapore 117543, the [§]Department of Neuroscience, Medical Faculty, University of Geneva, 1211 Geneva 4, Switzerland, the [¶]School of Medical Science, Griffith University Gold Coast Campus, Queensland 4222, Australia, the [‖]Department of Pharmacology, School of Medicine, National University of Singapore, Singapore 117597, and the **Department of Biochemistry and Molecular Biophysics, Medical College of Virginia, Virginia Commonwealth University, Richmond, Virginia 23298*

Snake venoms are a mixture of pharmacologically active proteins and polypeptides that have led to the development of molecular probes and therapeutic agents. Here, we describe the structural and functional characterization of a novel neurotoxin, haditoxin, from the venom of *Ophiophagus hannah* (King cobra). Haditoxin exhibited novel pharmacology with antagonism toward muscle ($\alpha\beta\gamma\delta$) and neuronal (α_7, $\alpha_3\beta_2$, and $\alpha_4\beta_2$) nicotinic acetylcholine receptors (nAChRs) with highest affinity for α_7-nAChRs. The high resolution (1.5 Å) crystal structure revealed haditoxin to be a homodimer, like κ-neurotoxins, which target neuronal $\alpha_3\beta_2$- and $\alpha_4\beta_2$-nAChRs. Interestingly however, the monomeric subunits of haditoxin were composed of a three-finger protein fold typical of curaremimetic short-chain α-neurotoxins. Biochemical studies confirmed that it existed as a non-covalent dimer species in solution. Its structural similarity to short-chain α-neurotoxins and κ-neurotoxins notwithstanding, haditoxin exhibited unique blockade of α_7-nAChRs (IC_{50} 180 nM), which is recognized by neither short-chain α-neurotoxins nor κ-neurotoxins. This is the first report of a dimeric short-chain α-neurotoxin interacting with neuronal α_7-nAChRs as well as the first homodimeric three-finger toxin to interact with muscle nAChRs.

Snake venoms are a rich source of pharmacologically active proteins and polypeptides targeting a variety of receptors with high affinity and specificity (1). Because of their high specificity, some of these molecules have contributed significantly (*a*) to the isolation and characterization of different receptors and their subtypes in the field of molecular pharmacology and (*b*) as lead compounds in the development of therapeutic agents (2, 3). For example, the discovery of α-bungarotoxin, a postsynaptic neurotoxin from the venom of *Bungarus multicinctus*, led to the identification of the nicotinic acetylcholine receptor (nAChR),[3] the first isolated receptor protein (4) as well as the first one to be characterized electrophysiologically (5) and biochemically (6, 7). Subsequently, it was also used to characterize several other nAChRs (8–10).

Snake venom proteins can be broadly classified as enzymatic and non-enzymatic proteins. Three-finger toxins (3FTxs) are the largest group of non-enzymatic snake venom proteins (1, 11). They are most commonly found in the venoms of elapid and hydrophiid snakes. Recently, our laboratory has also demonstrated the presence of 3FTxs from colubrid venoms (12, 13), and 3FTx transcripts have been found in the venom gland transcriptome of viperid snakes (14, 15). The proteins in this family of toxins share a common structural scaffold of three β-sheeted loops emerging from a central core (11, 16). Despite the overall similarity in structure, these proteins have diverse functional properties. Members of this family include neurotoxins targeting the cholinergic system (7, 11, 16), cytotoxins/cardiotoxins interacting with the cell membranes (17), calciseptine and related toxins that block the L-type Ca^{2+} channels (18), dendroaspins, which are antagonists of various cell adhesion processes (19), and β-cardiotoxin antagonizing the β-adrenoceptors (20). The subtle variations in their structures, such as the presence of extra disulfide bonds, differences in size and overall conformation (twists and turns) of the loops, and longer C-terminal and/or N-terminal extensions (21), may contribute to the observed functional diversity as well as specificity of these toxins (22).

* This work was supported by research grant from the Biomedical Research Council (BMRC), Agency for Science and Technology, Singapore (BMRC Grant R154-000-172-316) (to R. M. K.) and by Academic Research Fund funding support (Grant R154000438112) from National University of Singapore, Singapore (to J. S.).

◆ This article was selected as a Paper of the Week.

The atomic coordinates and structure factors (code 3HH7) have been deposited in the Protein Data Bank, Research Collaboratory for Structural Bioinformatics, Rutgers University, New Brunswick, NJ (http://www.rcsb.org/).

[S] The on-line version of this article (available at http://www.jbc.org) contains supplemental Fig. 1.

[1] Present address: ZMBH, University of Heidelberg, 69120 Heidelberg, Germeny.

[2] To whom correspondence should be addressed: Protein Science Laboratory, Dept. of Biological Sciences, Faculty of Science, National University of Singapore, Singapore 117543. Tel.: 65-6516-5235; Fax: 65-6779-2486; E-mail: dbskinim@nus.edu.sg.

[3] The abbreviations used are: nAChR, nicotinic acetylcholine receptor; mAChR, muscarinic acetylcholine receptors; 3FTx, three-finger toxin; MT, muscarinic toxin; BS^3, bis(sulfosuccinimidyl) suberate; CBCM, chick biventer cervicis muscle; RHD, rat hemidiaphragm muscle; r.m.s.d., root mean square deviation; RP-HPLC, reverse phase-high performance liquid chromatography; MS, mass spectrometry; ESI-MS, electrospray mass ionization-MS; Tricine, *N*-[2-hydroxy-1,1-bis(hydroxymethyl)ethyl]glycine; MTLP, muscarinic toxin-like protein.

This family contains several types of neurotoxins that interact with different subtypes of nicotinic and muscarinic receptors involved in central and peripheral cholinergic transmission. Depending on the target receptors, these neurotoxins can be broadly divided into various groups. Curaremimetic or α-neurotoxins that target muscle ($\alpha\beta\gamma\delta$ or α_1 subtype) nAChRs (7, 16, 23) belong to short-chain and long-chain neurotoxins (classified based on size and number of disulfide bridges (24)). Long-chain neurotoxins, but not short-chain neurotoxins, also target neuronal α_7-nAChRs associated with neurotransmission in the brain (25). κ-Neurotoxins, such as κ-bungarotoxin (*B. multicinctus*), show specificity for other neuronal subtypes, $\alpha_3\beta_2$- and $\alpha_4\beta_2$-nAChRs (26, 27). Muscarinic 3FTxs, unlike many small molecule ligands, can distinguish between different types of muscarinic acetylcholine receptors (mAChRs) (for review, see Ref. 28) and hence are useful in the characterization of these receptor subtypes. Muscarinic toxin 1, isolated from the venom of *Dendroaspis angusticeps*, interacts with mAChR subtype 1 (M1) (29), whereas muscarinic toxin 3 (MT3), isolated from the same snake, interacts with M4 mAChRs (30). In recent years, new 3FTxs with distinct and novel receptor specificities have been characterized and added to this growing library (12, 13, 31–36), justifying their usefulness as pharmacological tools to dissect the cholinergic circuitry to understand the role of individual receptor subtypes or offer clues to the rational design of specific therapeutics.

All neurotoxins characterized to date exist as monomers with the exception of κ-neurotoxins from *Bungarus* sp. (37, 38), which is a non-covalently linked homodimer that binds neuronal ($\alpha_3\beta_2$ and $\alpha_4\beta_2$) but not muscle ($\alpha\beta\gamma\delta$) nAChRs. More recently, we published the first report of a covalent heterodimeric neurotoxin, irditoxin from the venom of *Boiga* sp., which was a uniquely irreversible inhibitor of muscle ($\alpha\beta\gamma\delta$) nAChRs (13). Here, we report the purification, pharmacological characterization, and a high resolution crystal structure of a novel non-covalent homodimeric neurotoxin from the venom of *Ophiophagus hannah* (King cobra). Although its quaternary structure is similar to κ-neurotoxins, it exhibited novel pharmacology with potent blocking activity on muscle ($\alpha\beta\gamma\delta$) as well as neuronal (α_7, $\alpha_3\beta_2$, and $\alpha_4\beta_2$) nAChRs. Based on the high resolution crystal structure (1.55 Å) we have explored its structural similarities with other neurotoxins. This new toxin was named haditoxin (*O. hannah* dimeric neurotoxin) and is the first homodimeric three-finger neurotoxin interacting with α_1-nAChRs.

EXPERIMENTAL PROCEDURES

Materials—Lyophilized *O. hannah* venom was obtained from PT Venom Indo Persada (Jakarta, Indonesia) and Kentucky Reptile Zoo (Slade, KY). Reagents for N-terminal sequencing by Edman degradation are from Applied Biosystems (Foster City, CA). KCl, acetonitrile, and trifluoroacetic acid were from Merck KGaA, Darmstadt, Germany. Precision Plus protein standards, dual color (marker for SDS-PAGE), and bis(sulfosuccinimidyl) suberate (BS^3) were purchased from Bio-Rad Laboratories and Pierce, respectively. Superdex 30 HiLoad (16/60) column and Jupiter C18 (5 μ, 300 Å, 4.6 × 150 mm) were purchased from GE Healthcare and Phenomenex (Torrance, CA), respectively. Crystal screening solution and accessories were obtained from Hampton Research (Aliso Viejo, CA). All other chemicals including α-bungarotoxin from *B. multicinctus* were purchased from Sigma-Aldrich. All the reagents were of the highest purity grade. Water was purified using a MilliQ system (Millipore, Billerica, MA).

Animals—Animals (Swiss albino mice and Sprague-Dawley rats) were acquired from the National University of Singapore Laboratory Animal Center and acclimatized to the Department Animal Holding Unit for at least 3 days before the experiments. They were housed, four per cage, with food and water available *ad libitum* in a light controlled room (12-h light/dark cycle, light on at 7:00 a.m.) at 23 °C and 60% relative humidity. Domestic chicks (*Gallus gallus domesticus*) were purchased from Chew's Agricultural Farm, Singapore, and delivered on the day of experimentation. Animals were sacrificed by exposure to 100% carbon dioxide. All experiments were conducted according to the Protocol (021/07a) approved by the Institutional Animal Care and Use Committee of the National University of Singapore.

Purification of the Protein—*O. hannah* crude venom (100 mg dissolved in 1 ml of MilliQ water and filtered) was loaded onto a Superdex 30 gel filtration column, equilibrated with 50 mM Tris-HCl buffer; pH 7.4, and eluted with the same buffer using an ÄKTA purifier system (GE Healthcare). Fractions containing the toxin of interest were further subfractionated by reverse phase-high performance liquid chromatography (RP-HPLC) using a Jupiter C18 column, equilibrated with 0.1% (v/v) trifluoroacetic acid, and eluted with a linear gradient of 80% (v/v) acetonitrile in 0.1% (v/v) trifluoroacetic acid. Elution was monitored at 280 and 215 nm. Fractions were directly injected into an API-300 liquid chromatography-tandem MS system (PerkinElmer Life Sciences) to determine the mass and homogeneity of the protein as described previously (20). Analyte software (PerkinElmer Life Sciences) was used to analyze and deconvolute the raw mass data. Fractions showing the expected molecular mass were pooled and lyophilized.

Capillary Electrophoresis—Capillary electrophoresis was performed on a BioFocus3000 system (Bio-Rad) to determine the homogeneity of the protein after RP-HPLC. The native protein (1 μg/μl) was injected to a 25 μm × 17 cm coated capillary using a pressure mode (5 p.s.i./s) and run in 0.1 M phosphate buffer (pH 2.5) under 18 kV at 20 °C for 7 min. The migration was monitored at 200 nm.

N-terminal Sequencing—N-terminal sequencing of the native protein was performed by automated Edman degradation using a Procise 494 pulsed liquid-phase protein sequencer (Applied Biosystems) with an on-line 785A phenylthiohydantoin derivative analyzer. The phenylthiohydantoin amino acids were sequentially identified by mapping the respective separation profiles with the standard chromatogram.

CD Spectroscopy—Far-UV CD spectra (260–190 nm) were recorded using a Jasco J-810 spectropolarimeter (Jasco Corp., Tokyo, Japan) as described previously (20). The protein samples (concentration range 0.25–1 mg/ml) were dissolved in MilliQ water.

In Vivo Toxicity Study—Native protein (200 μl dissolved in 0.89% NaCl) was injected intraperitoneally using a 27-gauge 0.5-inch needle (BD Biosciences) into male Swiss albino mice (15 ± 2 g) at doses of 5, 10, and 25 mg/kg ($n = 2$). The symptoms of envenomation were observed, and in the event of death, the time of death was noted. The control group was injected with 200 μl of 0.89% NaCl. Postmortem examinations were conducted on all animals.

Ex Vivo Organ Bath Studies—Isolated tissue experiments were performed as described previously (13, 31) using a conventional organ bath (6 ml) containing Krebs solution of the following composition (in mM): 118 NaCl, 4.8 KCl, 1.2 KH_2PO_4, 2.5 $CaCl_2$, 25 $NaHCO_3$, 2.4 $MgSO_4$, and 11 D-(+)glucose); pH 7.4, at 37 °C. This is continuously aerated with carbogen (5% carbon dioxide in oxygen). The resting tension of the tissues was maintained at 1–2 g, and the preparations were allowed to equilibrate for 30–45 min. Electrical field stimulation was carried out through platinum ring electrodes using a Grass stimulator S88 (Grass Instruments, West Warwick, RI). The magnitude of the contractile response was measured in gram tension. Data were continuously recorded on PowerLab/Chart 5 data acquisition system via a force displacement transducer (Model MLT0201) (AD Instruments, Bella Vista NSW, Australia). Neuromuscular blockade produced by a toxin is expressed as a percentage of the original twitch height in the absence of exposure to toxin. Dose-response curves representing the percent blockade after 30 min of exposure to the respective toxins were plotted.

Chick Biventer Cervicis Muscle (CBCM) Preparations—The CBCM nerve-skeletal muscle preparation (39) was isolated from chicks (6 days old) and mounted in the organ bath chamber under similar experimental conditions as described previously (12, 31). The effect of haditoxin (0.05–5 μM; $n = 3$) or α-bungarotoxin (0.01–1.0 μM; $n = 3$) on nerve-evoked twitch responses of the CBCM were studied. In separate experiments, the recovery from complete neuromuscular blockade was assessed by washing out the toxin with Krebs solution at 30-min intervals (three cycles of 30-s on pulse, 30-s off pulse) over a 120-min period.

Rat Hemidiaphragm Muscle (RHD) Preparations—The RHD muscle associated with the phrenic nerve (40) was isolated and mounted in a 5-ml organ bath chamber under similar conditions as stated for CBCM, as described previously (13). The effects of haditoxin (0.15–15 μM; $n = 3$) or α-bungarotoxin (0.01–1.0 μM; $n = 3$) on nerve-evoked twitch responses of the RHD were investigated. Recovery of neuromuscular blockade was assessed similarly as described above for CBCM.

Electrophysiology—Two-electrode voltage clamp experiments were done using *Xenopus* oocytes. The oocytes were prepared and injected as described by Hogg *et al.* (41). Briefly, 2 ng of cDNA encoding for human $\alpha_4\beta_2$-, $\alpha\beta\delta\epsilon$-, α_7-, and $\alpha_3\beta_2$-nAChRs were injected into the oocytes. Two-electrode voltage clamp measurements were done 2–3 days after injection. During recordings, the oocytes were perfused with OR2 (oocyte ringer) containing (in mM): 82.5 NaCl, 2.5 KCl, 1 $MgCl_2$, 2.5 Ca_2Cl, 5 HEPES, and 20 μg/ml bovine serum albumin; pH 7.4. Atropine (0.5 μM) was added to all solutions to block activity of endogenous muscarinic receptors. Just before use, acetylcholine (ACh) and haditoxin were dissolved the OR2 solution. All recordings were performed with an automated two-electrode voltage clamp robot. Oocytes were clamped at −100 mV, and data were digitized and analyzed off-line using MATLAB (Mathworks, Natick, MA).

Gel Filtration Chromatography—The oligomeric states of the protein were examined by gel filtration chromatography on a Superdex 75 column (1 × 30 cm) equilibrated with 50 mM Tris-HCl buffer (pH 7.4) using an ÄKTA purifier system at a flow rate of 0.6 ml/min. Calibration was done using bovine serum albumin (66 kDa), carbonic anhydrase (29 kDa), cytochrome *c* (12.4 kDa), aprotinin (6.5 kDa), and blue dextran (200 kDa) as molecular mass markers. Native protein (0.25–10 μM) as well as samples (0.25–10 μM) treated with 0.6% SDS (2 h of incubation at room temperature) (37) were loaded separately onto the column, and respective elution profiles were recorded. For the SDS-treated samples, the column was equilibrated with the same buffer containing 0.1% SDS.

Electrophoresis—Tris-Tricine SDS-PAGE of the protein of interest in the presence or absence of cross-linker BS^3 (42) was performed on a 12% gel, under reducing conditions, using the Bio-Rad Mini-Protean II electrophoresis system. The concentration of BS^3 used was 5 mM. The protein bands were visualized by Coomassie Blue staining.

Crystallization and Data Collection—Crystallization conditions for the protein were screened with Hampton Research screens using the hanging-drop vapor diffusion method. Lyophilized protein was dissolved in 10 mM Tris-HCl buffer, pH 7.4, with 100 mM NaCl. Crystallization experiments were performed at room temperature 297 K (24 °C) with drops containing equal volumes (1 μl) of reservoir and protein solution. Small rod-shaped crystals were formed within 2–3 days and grew to diffraction quality after 3 weeks. They were briefly soaked in the reservoir solution supplemented with 10% glycerol as cryo-protectant prior to the x-ray diffraction data collection. Then these were flash-frozen in a nitrogen cold stream at 100 K (−173 °C). Diffraction up to 1.55 Å was obtained using a CCD detector (Platinum135) mounted on a Bruker Microstar Ultra rotating anode generator (Bruker AXS, Madison, WI). A complete data set was collected, processed, and scaled using the program HKL2000 (43).

RESULTS

Five novel 3FTxs were identified from the cDNA library of the venom gland tissue of *O. hannah*, and one of them, named β-cardiotoxin, has been characterized previously (20). Here, we describe the characterization of the second novel toxin, identified previously as an MTLP-3 homolog based on sequence homology (20) (Fig. 1). The liquid chromatography/MS profile of *O. hannah* venom (44) showed the presence of a 7,535.67 ± 0.60 Da protein, similar to the expected molecular mass of the protein being characterized. This protein was purified from the crude venom using a two-step chromatographic approach. Firstly, the venom components were separated based on their sizes into five peaks using gel filtration chromatography (Fig. 2*A*). Subsequently, each peak was fractionated by RP-HPLC, and the fractions were analyzed by ESI-MS to identify the presence of the protein of interest (Fig. 2*A*, *black bar*). Further, these

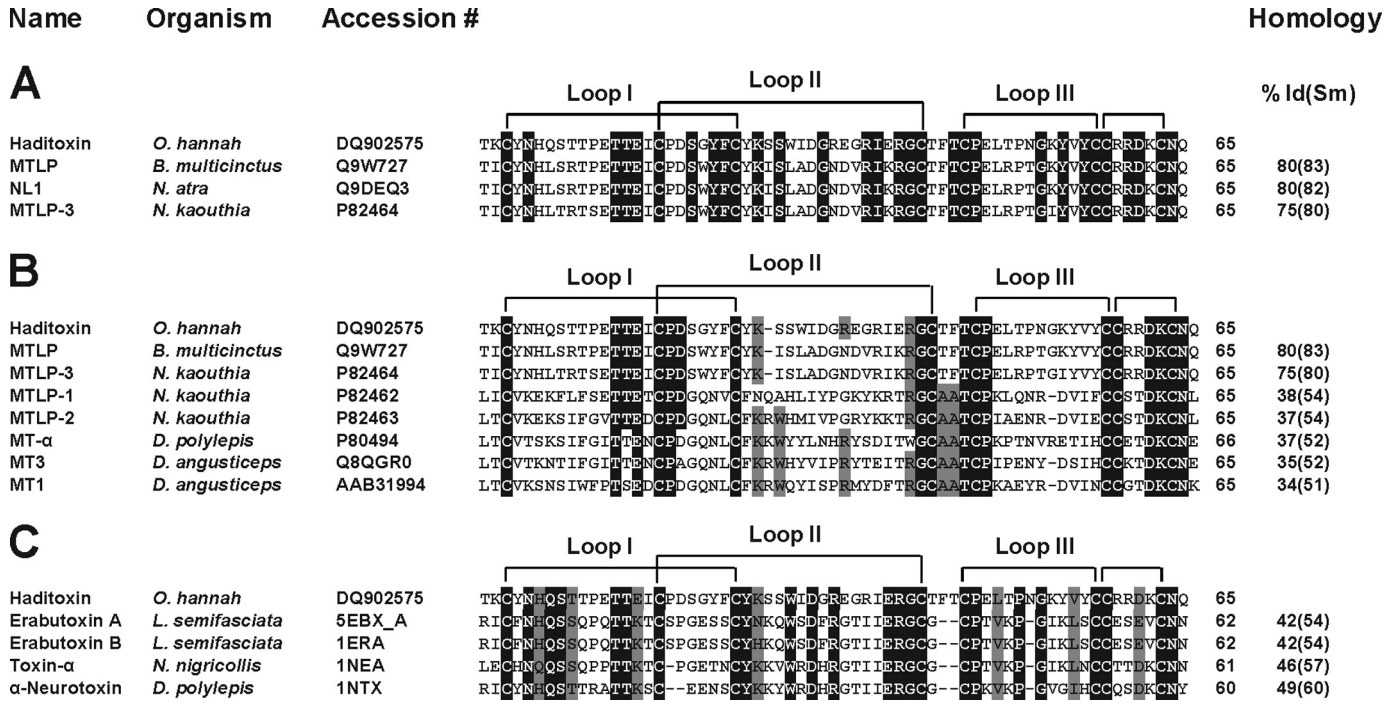

FIGURE 1. **Multiple sequence alignment of novel proteins.** *A–C*, sequence alignment of haditoxin with the most homologous sequences (*A*), muscarinic toxin homologs (*B*), and short-chain α-neurotoxins (*C*). Toxin names, species, and accession numbers are shown. Conserved residues in all sequences are highlighted in *black*. Disulfide bridges and loop regions are also shown. At the end of each sequence, the numbers of amino acids are stated. The homology (sequence identity and similarity (*% Id(Sm)*)) of each protein is compared with haditoxin and shown at the end of each sequence. *N. atra*, *Naja atra*; *N. kaouthia*, *Naja kaouthia*; *D. polylepis*, *Dendroaspis polylepis*; and *L. semifasciata*, *Laticauda semifasciata*.

fractions were pooled and separated by RP-HPLC (Fig. 2*B*). The ESI-MS of fraction 2a (Fig. 2*C*, *black arrow*) showed three peaks with mass/charge (*m*/*z*) ratios ranging from +4 to +6 charges (Fig. 2*C*), and the final reconstructed mass spectrum showed a molecular mass of 7,535.67 ± 1.25 Da, which matched the calculated mass of 7,534.42 Da (Fig. 2*C*, *inset*). The secondary structural elements of haditoxin were analyzed using far-UV CD spectroscopy. The spectrum shows maxima at 230 and 198–200 nm and a minimum at 215 nm (Fig. 2*D*). Thus, haditoxin was found to be composed of β-sheeted structure similar to all other 3FTxs (11, 16). The presence of a single protein peak in the electropherogram (Fig. 2*E*) indicates the homogeneity of the protein, ensuring the absence of contaminants, especially other α-neurotoxin(s) and cytotoxins present in the venom. Identification was further confirmed by N-terminal sequencing of the first 36 residues, which matched the cDNA sequence of the MTLP-3 homolog (20). This protein was found to be a homodimer (see below) and hence was renamed as haditoxin (*O. hannah* dimeric neurotoxin) following the nomenclature of dimeric 3FTxs (12, 13).

Investigation of Haditoxin for Muscarinic Effects—As detailed in Fig. 1, *A* and *B*, haditoxin showed high similarity (80–83%) with muscarinic toxin homologs (MTLP and MTLP-3) as well as similarity with muscarinic toxins (MT-α, MT7, and MT3) (51–52%). As such, we examined the effects of haditoxin on *in vitro* smooth muscle preparations, the rat ileum and rat anococcygeus muscle, pharmacologically characterized to represent M2 (45) and M3 mAChRs (46), respectively. In both preparations, the protein had no effect on the contractile response of the muscle to exogenously applied ACh or electrical field stimulation, suggesting that haditoxin does not interact with M2 and M3 mAChRs (supplemental Fig. 1). Therefore, it is likely that the observed sequence similarity with muscarinic toxin homologs is probably coincidental due to either phylogeny or structure, including the presence of the core disulfide bridges, and not the function. This merits further investigation, including electrophysiological studies and/or binding assays on other subtypes of mAChRs.

In Vivo Toxicity of Haditoxin—In preliminary experiments to observe the biological effects of haditoxin, all mice injected with the toxin (5, 10, and 25 mg/kg) showed typical symptoms of peripheral neurotoxicity, such as paralysis of hind limbs and labored breathing, and finally died, presumably due to respiratory paralysis (47, 48). The time of death was recorded for each animal, with the average calculated to be 94, 32.5, and 20 min, respectively, for the 5, 10, and 25 mg/kg doses. On postmortem, no gross changes in the internal organs, notably hemorrhage, were observed.

Ex Vivo Neurotoxic Effects of Haditoxin—The observed peripheral neurotoxic symptoms produced by haditoxin *in vivo* warranted detailed pharmacological characterization on neuromuscular transmission using CBCM and RHD preparations. Haditoxin (1.5 μM) produced a reproducible time- and dose-dependent neuromuscular blockade in both preparations (Fig. 3, *A* and *C*). In the CBCM, it completely inhibited the contractile response to exogenous agonists (ACh and carbachol (*CCh*)), whereas response to exogenous KCl and twitches evoked by direct muscle stimulation were not inhibited, indicating a postsynaptic neuromuscular blockade and an absence of direct myotoxicity.

The IC_{50} of haditoxin on CBCM and RHD was 0.27 ± 0.07 and 1.85 ± 0.39 μM, respectively (Fig. 3*E*) (considering the fact

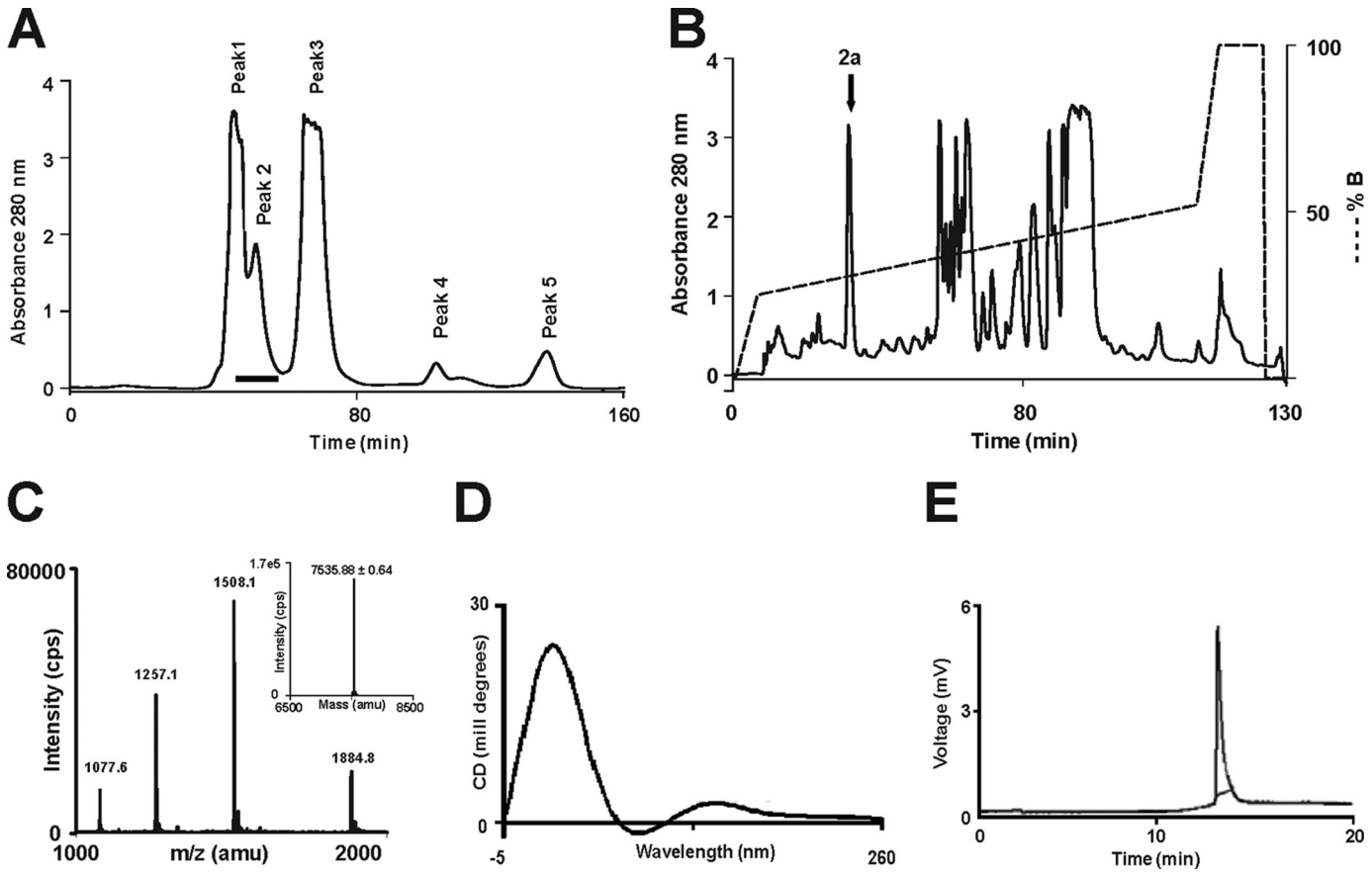

FIGURE 2. **Purification of haditoxin from the venom of *O. hannah*.** *A*, gel filtration chromatogram of crude venom. Crude venom (100 mg/ml) was fractionated using a Superdex 30 HiLoad (16/60) column. The column was pre-equilibrated with 50 mM Tris-HCl buffer (pH 7.4). Proteins were eluted at a flow rate of 1 ml/min using the same buffer. A *black bar* at *Peak 2* indicates the fractions containing haditoxin. *B*, RP-HPLC profile of the gel filtration fractions containing haditoxin. Jupiter C18 (5 μ, 300 Å, 4.5 × 250 mm) analytical column was equilibrated with 0.1% (v/v) trifluoroacetic acid. Protein of interest was eluted from the column with a flow rate of 1 ml/min with a gradient of 23–49% buffer B (80% acetonitrile in 0.1% trifluoroacetic acid). The *dotted line* indicates the gradient of the buffer B. The *downward arrow* at *Peak 2a* indicates fractions containing haditoxin. *C*, ESI-MS profile of the RP-HPLC fraction containing haditoxin. The spectrum shows a series of multiply charged ions, corresponding to a single, homogenous peptide with a molecular mass of 7,535.88 Da. *Inset*, reconstructed mass spectrum of haditoxin; *CPS* = counts/s; *amu* = atomic mass units. *D*, far-UV CD spectrum of haditoxin. The protein was dissolved in MilliQ water (0.5 mg/ml), and the CD spectra were recorded using a 0.1-cm path length cuvette. *E*, electropherogram of haditoxin. The sample was injected using pressure mode 5 p.s.i./s, and electrophoresis runs were carried out using a coated capillary (17 cm × 25 μm) at 18 kV, with 0.1 M phosphate buffer (pH 2.5) at 20 °C for 7 min.

that the protein exists as dimer in solution; see below). When compared with α-bungarotoxin (IC_{50} on CBCM 12.1 ± 5.4 nM and RHD 100.5 ± 22.5 nM) (Fig. 3*E*), haditoxin was about 50 times less potent on both avian (CBCM) and mammalian (RHD) neuromuscular junctions.

Reversibility of the neuromuscular blockade was tested for both preparations with intermittent washing (Fig. 3, *D* and *F*, *black arrows*). Partial recovery of the contractile response (60% recovery in 2 h) was observed in the CBCM (Fig. 3*B*) but not in the RHD (Fig. 3*D*). These results indicate that unlike typical α-neurotoxins such as α-bungarotoxin, haditoxin exhibits partial reversibility in action, at least in the CBCM.

Effect of Haditoxin on Human nAChRs—Because haditoxin blocked the muscle activity of the CBCM and RHD, we examined its activity on human αβδε-nAChRs. Haditoxin completely inhibited the ACh-induced αβδε currents at a concentration of 10 μM (Fig. 4*A*) with an IC_{50} value of 550 nM ($n = 13$) (Fig. 4*B*). This inhibition was practically irreversible within 8 min of washout. This result is in good agreement with the findings on e*x vivo* studies with RHD as discussed earlier. Next, we tested the activity of haditoxin on α_7- and $\alpha_3\beta_2$-nAChRs. On α_7-nAChRs, an irreversible block was observed at 10 μM concentration of haditoxin (Fig. 4*C*) with an IC_{50} value was 180 nM ($n = 4$) (Fig. 4*D*). As shown in Fig. 4*E*, 10 μM haditoxin fully blocked the response of $\alpha_3\beta_2$-nAChRs, with an IC_{50} value of 500 nM ($n = 4$) (Fig. 4*F*). Notably, the blockade at $\alpha_3\beta_2$ was fully reversible, whereas long-lasting blockade was observed at α_7-nAChRs. This suggests that the K_{Off} value at the α_7 receptor is much smaller than at $\alpha_3\beta_2$-nAChRs. As these two receptors display about equivalent IC_{50} values, this indicates that their respective K_{On} values are probably significantly different. However, the experimental protocol used herein prevents the detailed analysis of the K_{On} and K_{Off} values. An additional difference between these two receptors resides in their structural composition. Although it is thought that α_7-nAChRs display five identical ligand binding sites, only two binding sites are proposed for the $\alpha_3\beta_2$-nAChRs. The difference in number of binding sites and effects on competitive blockade was previously discussed for α_7- and $\alpha_4\beta_2$-nAChRs, showing significant functional outcomes (49). Interestingly, haditoxin was almost 3-fold more potent to block ACh-induced responses mediated by α_7-nAChRs (IC_{50} = 180 nM, $n = 4$) when compared with

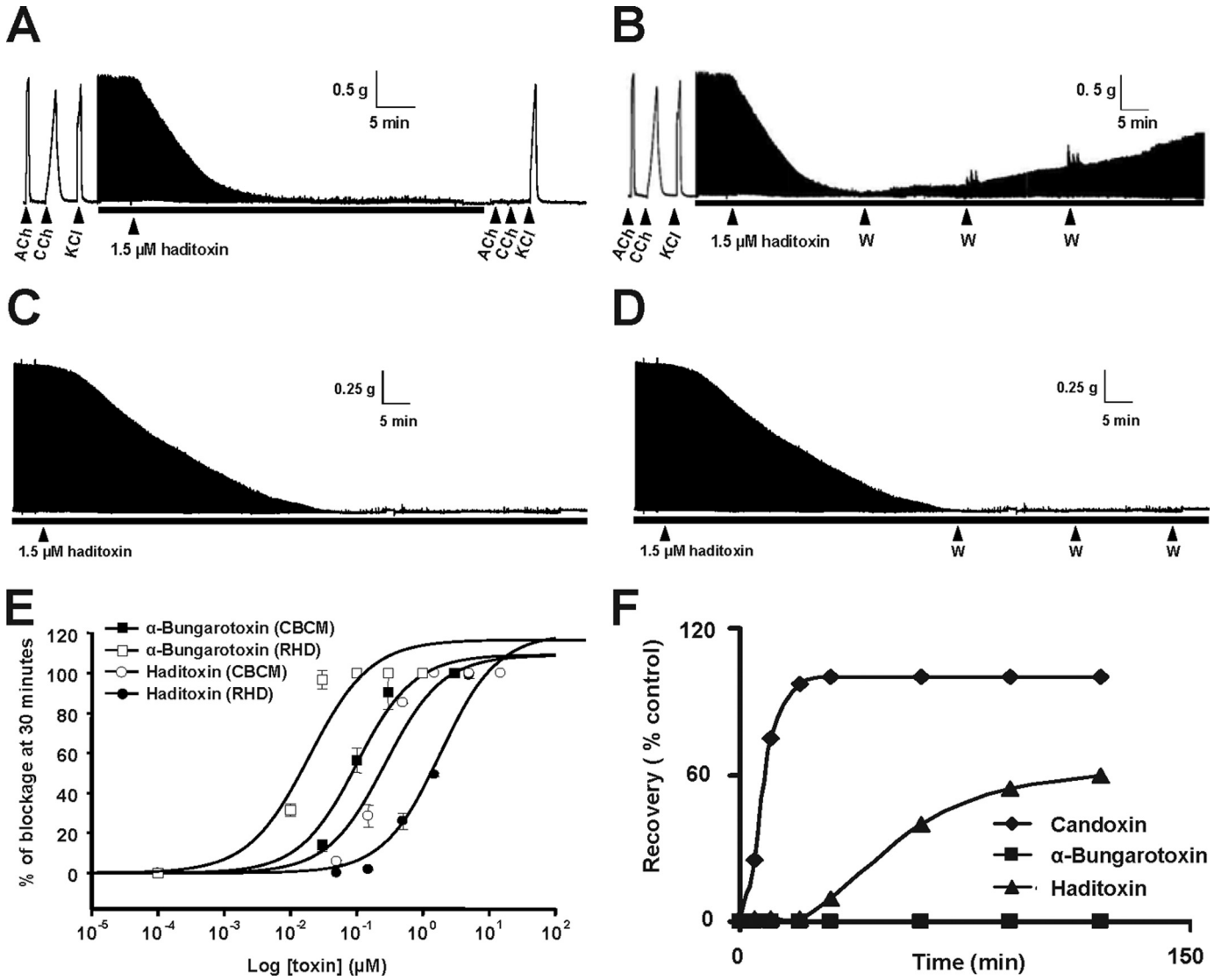

FIGURE 3. **Pharmacological profile of haditoxin.** *A–D*, a segment of tracing showing the effect of haditoxin (1.5 μM) on CBCM preparations (*A*), reversibility of CBCM preparation (*B*), RHD preparations (*C*), and reversibility of RHD preparation (*D*). Contractions were produced by exogenous ACh (300 μM), carbachol (*CCh*; 10 μM), and KCl (30 mM). The *black bar* indicates the electrical field stimulation. The point of washing out the toxin with Krebs solution in reversibility studies is indicated by the abbreviation *W*. *E*, dose-response curve of haditoxin and α-bungarotoxin on CBCM and RHD. The block is calculated as a percentage of the control twitch responses of the muscle to supramaximal nerve stimulation. Each data point is the mean ± S.E. of at least three experiments. *F*, comparative reversibility profile of α-bungarotoxin, haditoxin, and candoxin.

$\alpha\beta\delta\epsilon$- and $\alpha_3\beta_2$-nAChRs. There was no recovery after application of haditoxin. Finally, we tested the effect of haditoxin on $\alpha_4\beta_2$-nAChRs. Application of 10 μM haditoxin blocked only 70% of the current with partial reversibility (Fig. 4*G*). The IC_{50} value of the blockade is in the micromolar range (IC_{50} = 2.6 μM, n = 3) (Fig. 4*H*). However, further experiments will be necessary to discriminate between the different mechanisms of blockade and recovery. These results show that haditoxin had a higher potency for α_7-nAChRs than for the other nAChRs. IC_{50} values for $\alpha\beta\delta\epsilon$- and $\alpha_3\beta_2$-nAChRs were in the same nanomolar range, whereas for $\alpha_4\beta_2$-nAChRs, it was in the micromolar range.

Haditoxin Is a Dimer—During the gel filtration of the crude venom, we observed that haditoxin eluted earlier when compared with other 3FTxs (Fig. 2*A*, most of the 3FTxs elutes in *Peak 3*). This led us to investigate the oligomeric states of this protein. Thus, we carried out analytical gel filtration experiments using a Superdex G-75 column. Protein, at concentrations (0.25–10 μM) covering the IC_{50} in CBCM (0.27 ± 0.07 μM) and RHD (1.85 ± 0.39 μM) preparations, was loaded onto the column. At all of these concentrations, the presence of a single peak corresponding to a relative molecular mass of 16.25 kDa was observed (Fig. 5*A*), supporting the existence of a dimeric species. To observe the effect of SDS on dimerization, we treated the protein (0.25–10 μM) with SDS and eluted using the same column. It eluted as a single peak with a M_r of 8.16 kDa (Fig. 5*A*), similar to the monomeric species.

The dimerization was further confirmed by Tris-Tricine SDS-PAGE analysis in the presence and absence of a cross-linker, BS^3 (Fig. 5*B*). In the presence of BS^3, both the dimeric and the monomeric species were visualized (Fig. 5*B*, *lane 1*), whereas only the monomeric species were observed in its absence (Fig. 5*B*, *lane 2*). These results, together with MS data (showing monomeric mass, Fig. 2*C*), indicate the existence of

haditoxin as a homodimer in solution at pharmacologically relevant concentrations, and the dimerization occurs through non-covalent interactions. Further, as haditoxin loses its β-sheeted structure and becomes random coil in the presence of SDS (as indicated by CD studies; data not shown), its overall conformation may play a critical role in the dimerization.

Crystal Structure of Haditoxin—To determine the three-dimensional structure of haditoxin, we used the x-ray crystallographic method. Diffraction quality crystals of haditoxin were obtained with 0.1 M Tris, pH 8.5, 20% v/v ethanol (Hampton Research crystal screen 2, condition 44). Diffraction up to 1.55 Å was observed, and the crystals belonged to the space group $P2_1$ (Table 1).

Structure Determination and Refinement—The structure of haditoxin was solved by the molecular replacement method (Molrep) (50). Initially, toxin-α, isolated from *Naja nigricollis* venom, was used as a search model (Protein Data Bank (PDB) code 1IQ9; sequence identity ~48%). The rotation and translation resulted in a correlation factor of 0.07 and R_{cryst} of 0.57. Further minimization in Refmac (51) reduced the *R* factor to 0.42. An excellent quality electron density map was calculated at this stage, which allowed us to auto-build 90% of the haditoxin model with ARP/wARP (52). The resulting model with the electron density map was examined to manually build the rest of the model using the Coot program (53). After a few cycles of map fitting and refinement, we obtained an *R* factor of 0.194 (R_{free} = 0.225) for reflections $I > \sigma I$ within 20-1.55 Å resolution. Throughout the refinement (Table 1), no noncrystallographic symmetry restraint was employed. All 65 residues (considering one subunit) are well defined in the electron density map (Fig. 6*A*), and statistics for the Ramachandran plot using PROCHECK (54) showed the presence of 88.9% of non-glycine residues in the most favored region.

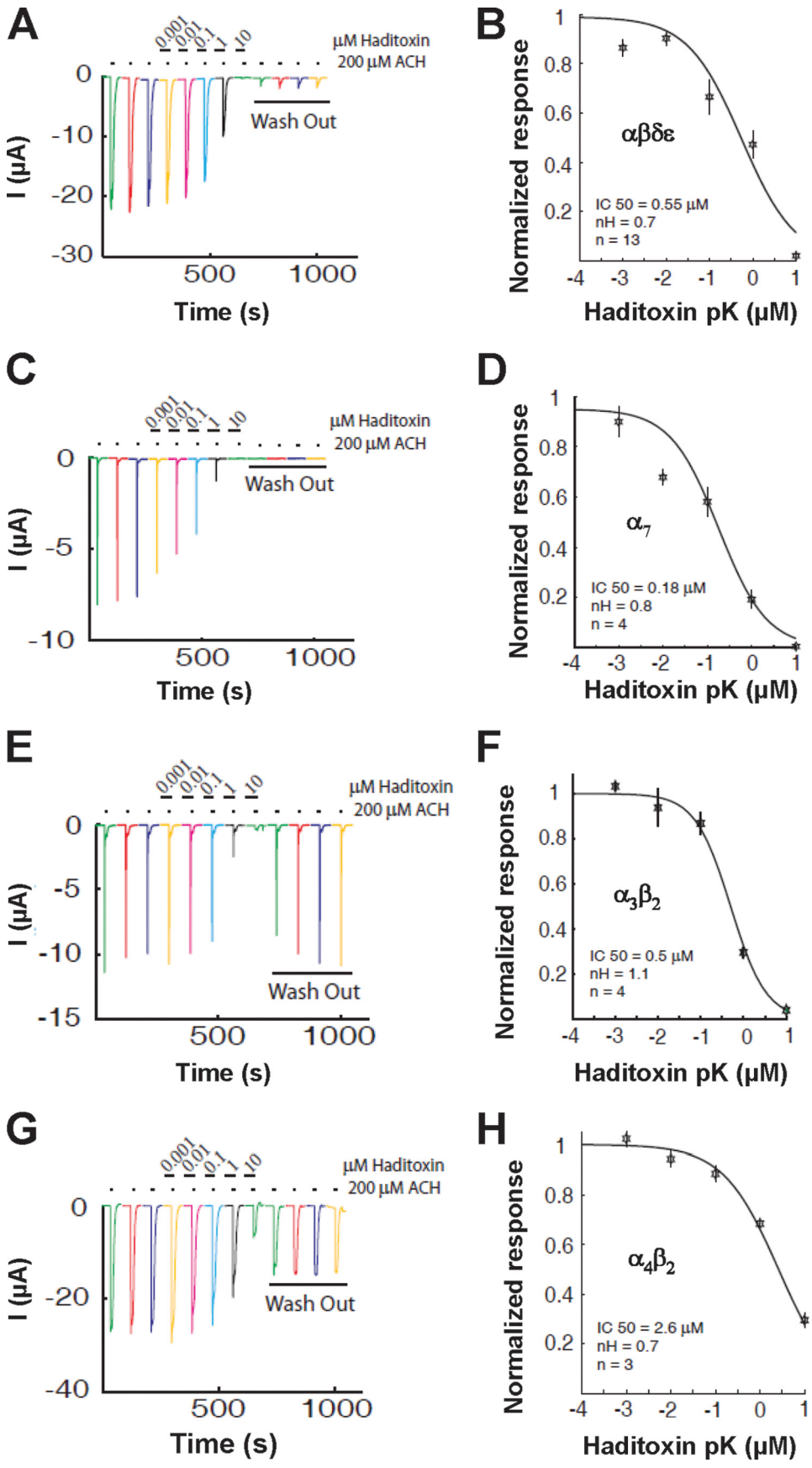

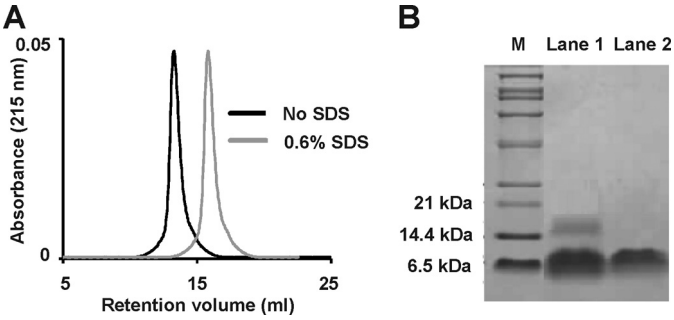

FIGURE 5. **Dimerization of haditoxin.** *A*, gel filtration profile of haditoxin with (*gray*) and without (*black*) SDS. 1 μM haditoxin was loaded onto a Superdex 75 column (1 × 30 cm) equilibrated with 50 mM Tris-HCl buffer (pH 7.4). The protein was eluted out with the 50 mM Tris-HCl buffer (pH 7.4) or 50 mM Tris-HCl buffer (pH 7.4) containing 0.6% SDS at flow rate of 0.6 ml/min. *B*, Tris-Tricine SDS-PAGE analysis of haditoxin with (*lane 1*) and without (*lane 2*) cross linker (BS^3). *M* is the marker lane. The concentration of BS^3 is 5 mM.

TABLE 1
X-ray data collection and refinement statistics

Data collection	
Cell parameters (Å)	$a = 37.27$, $b = 41.29$, $c = 40.98$, $\beta = 106.4°$
Space group	$P2_1$
Molecules/asymmetric unit	2
Resolution range (Å)	50–1.55
Wavelength (Å)	1.5418
Observed reflections	82,388
Unique reflections	17,366
Completeness (%)	99.1 (92.9)
R_{sym} (%)[a]	0.093
$I/\sigma(I)$	40.2 (6.0)
Refinement and quality	
Resolution range (Å)	20–1.55
R_{work} (%)[b]	19.4
R_{free} (%)[c]	22.5
r.m.s.d. bond lengths (Å)	0.009
r.m.s.d. bond angles (deg)	1.274
Average *B* factors (Å^2)	15.1
Number of protein atoms	1408
Number of waters	114
Ramachandran plot (%)	
Most favored regions	88.9
Additional allowed regions	9.3
Generously allowed regions	1.9
Disallowed regions	0

[a] $R_{sym} = \sum|I_i - \langle I\rangle|/\sum|I|$, where I_i is the intensity of the *i*th measurement, and $\langle I\rangle$ is the mean intensity for that reflection.
[b] $R_{work} = \sum||F_{obs}| - |F_{calc}||/\sum|F_{obs}|$, where F_{calc} and F_{obs} are the calculated and observed structure factor amplitudes, respectively.
[c] R_{free} = as for R_{work}, but for 10% of the total reflections chosen at random and omitted from refinement.

The coordinates and structure factors have been deposited with the Research Collaboratory for Structural Bioinformatics (RCSB) PDB (55) with the code 3HH7. The asymmetric unit consists of two monomers forming a tight dimer having an approximate dimension of 25 × 13 × 4 Å (Fig. 6*B*). This crystallographic dimer is consistent with the gel filtration and SDS-PAGE observations (Fig. 5). Both monomers are related by a two-fold symmetry, and their superposition yielded an r.m.s.d. of 0.2 Å for 65 Cα atoms (Fig. 7*A*). Each monomer adopts the common three-finger fold (11) consisting of three β-sheeted loops protruding from a central core, tightened by four highly conserved disulfide bridges (Cys-3–Cys-24, Cys-17–Cys-41, Cys-45–Cys-57, and Cys-58–Cys-63) (Fig. 6, *B* and *C*), and are structurally similar to short-chain α-neurotoxins such as toxin-α and erabutoxins (Fig. 7*B*). Loop I forms a two-stranded β-sheet (Lys-2–Tyr-4 and Thr-14–Ile-16), whereas loops II and III form a three-stranded β-sheet (Glu-34–Thr-42, Phe-23–Asp-31, and Lys-53–Cys-58). The antiparallel β-strands of the β-sheet are stabilized by main chain-main chain hydrogen bonding.

Dimeric Interface—The dimeric interface was analyzed using the Protein Interfaces, Surfaces and Assemblies (PISA) server (56). It is mainly formed by loop III of each subunit. Strands D, C, E, E′, C′, and D′ form a six β-pleated sheet with an overall right-handed twist (Fig. 6*B*) in the dimer. Approximately 565 Å^2 (or 12% of the total) surface areas and 17 residues of each monomer contribute to the dimerization. The close contacts between the monomers are maintained by 14 hydrogen bonds (<3.2 Å) and extensive hydrophobic interactions (Table 2). Six main chain-main chain hydrogen-bonding contacts exist across the interface involving strand E of monomer A and E′ of B (Table 2, Fig. 7*C*). Four are observed between the main chain amide hydrogen and carbonyl oxygen of Val-55 and Cys-57 from monomer A and Val-55′ and Cys-57′ from monomer B, and the remaining two exist between the carbonyl oxygen of Lys-53 (and Lys-53′) and the amide hydrogen of Arg-59 (and Arg-59′). In addition, there are another eight hydrogen-bonding contacts mediated through the side chains of Thr-44, Cys-45, Glu-47, Pro-50, and Arg-59 (Table 2, Fig. 7*C*). Two hydrophobic clusters further stabilize the dimeric structure. The side chains of Phe-23 and Leu-48 from both monomers form one cluster, whereas the disulfide bridge between Cys-45–Cys-57 and Val-55 of both monomers form the other. These observations strongly suggest the existence of haditoxin as non-covalent homodimeric species.

DISCUSSION

Nonenzymatic neurotoxins from snake venom belonging to the 3FTx family consist of closely related polypeptides with a molecular mass range of 6,500–8,000 Da. Functionally, most interfere with cholinergic neurotransmission and are highly specific for different subtypes of muscarinic or nicotinic cholinergic receptors (for details, see the Introduction). This underscores their immense potential as lead molecules in drug discovery and as research tools in the characterization of receptor subtypes.

Here, we have described the purification and characterization of a novel neurotoxin, haditoxin, from the venom of *O. hannah*. It is a non-covalent homodimer that produces potent postsynaptic neuromuscular blockade of the mammalian muscle (IC_{50} = 1.85 ± 0.39 μM) and avian muscle (IC_{50} = 0.27 ± 0.07 μM) ($\alpha\beta\gamma\delta$)

FIGURE 4. **Effect of haditoxin on human nAChRs expressed in *Xenopus* oocytes.** *A*, *C*, *E*, and *G*, inhibition of ACh-induced currents in $\alpha\beta\delta\epsilon$- (neuromuscular junction) (*A*), α_7- (*C*), $\alpha_4\beta_2$- (*E*), and $\alpha_3\beta_2$-nAChRs (*G*). Neuromuscular junction currents were activated by 10 μM ACh, whereas 200 μM was used to activate α_7-, $\alpha_4\beta_2$-, and $\alpha_3\beta_2$-nAChRs. The first three traces are controls, followed by a 2-min exposure to several haditoxin concentrations ranging from 10 nM to 10 μM. Each experiment was terminated by a 8-min wash out. Little or no recovery was observed for $\alpha\beta\delta\epsilon$- and α_7-nAChRs, whereas partial to full recovery was observed for $\alpha_4\beta_2$- and $\alpha_3\beta_2$-nAChRs. Inhibition curves of the fitted data, IC_{50}, and Hill coefficient (*nH*) for $\alpha\beta\delta\epsilon$-nAChRs (*B*) were 0.55 μM and 0.7; for α_7-nAChRs (*D*), they were 0.18 μM and 0.8; for $\alpha_3\beta_2$-nAChRs (*F*), they were 0.5 μM and 1.1; and for $\alpha_4\beta_2$-nAChRs (*H*), they were 2.6 μM and 0.7. *Error bars* indicate S.E.

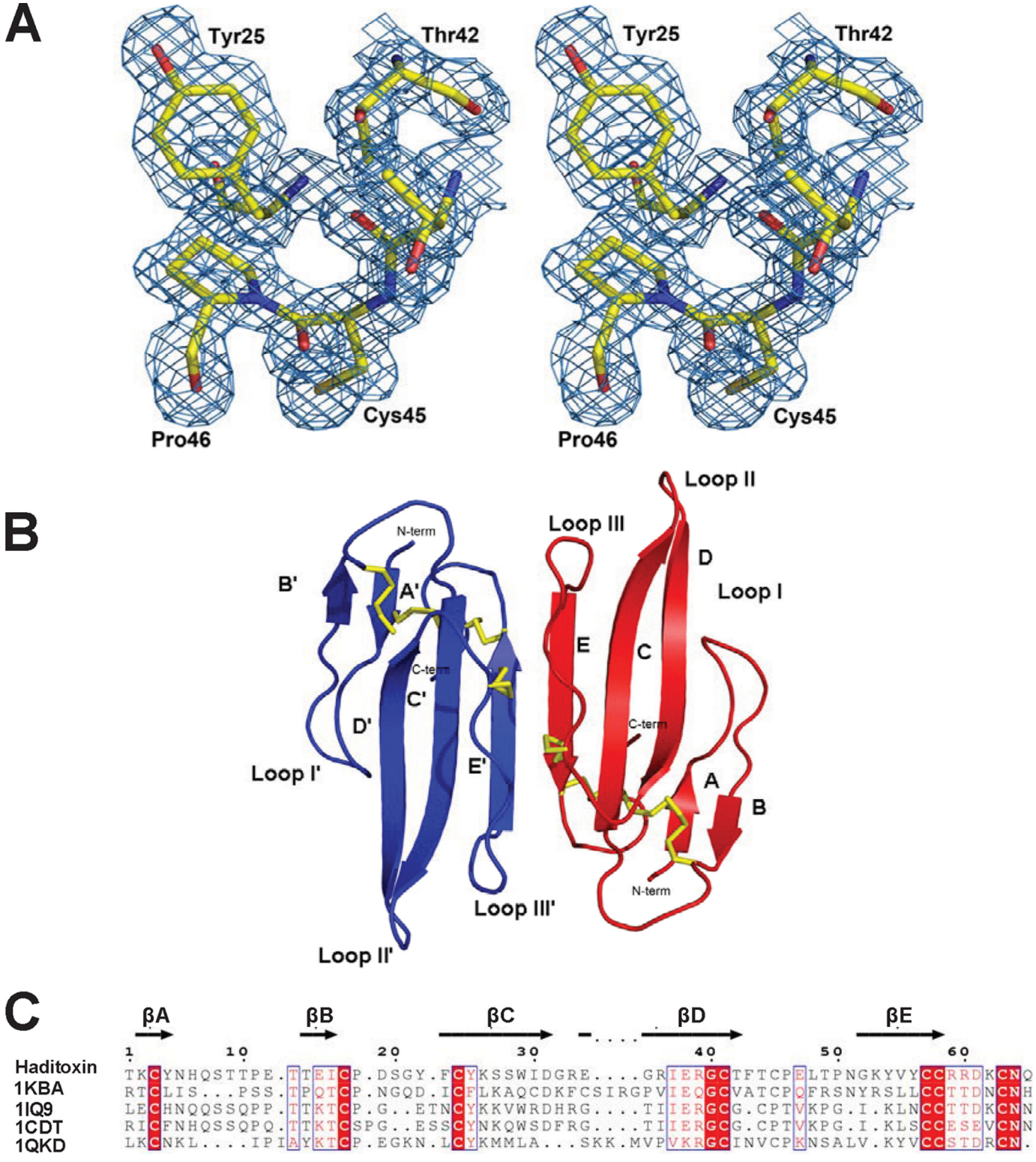

FIGURE 6. **Overall structure of haditoxin.** *A*, stereo view of a portion of the final $2F_o - F_c$ map of haditoxin. The map was contoured at a level of 1.0 σ. *B*, monomers A and B are shown in *blue* and *red*, respectively. Disulfide bonds are shown in *yellow*. N and C termini (*N-term* and *C-term*), β-strands, and loops I, II, and III are labeled. *C*, structure-based alignment of three-finger toxins. Color coding of conserved residues is provided by *boxed red text*, and color coding of invariant residues is provided by *red highlight*. Accession numbers are shown on the *left*, and secondary structural elements of haditoxin are shown on *top*. Numbering is shown for haditoxin only. Sequence alignment was done by Strap (82) and displayed with ESPript (83).

nAChRs (Fig. 3, *A* and *C*). In electrophysiological studies, it was an antagonist of muscle ($\alpha\beta\delta\epsilon$) ($IC_{50}$ = 0.55 μM) as well as neuronal α_7- (IC_{50} = 0.18 μM), $\alpha_3\beta_2$- (IC_{50} = 0.50 μM), and $\alpha_4\beta_2$- (IC_{50} = 2.60 μM) nAChRs (Fig. 4). Interestingly, haditoxin exhibited a novel pharmacology with combined blocking activity on muscle ($\alpha\beta\gamma\delta$) as well as neuronal (α_7, $\alpha_3\beta_2$, and $\alpha_4\beta_2$) nAChRs but with the highest potency on α_7-nAChRs, which is recognized by neither short-chain α-neurotoxins nor κ-neurotoxins.

The reversibility of this neuromuscular blockade was taxa-specific; it is partially reversible by washing in the chick neuromuscular junction, whereas it was almost irreversible in the rat neuromuscular junction. Earlier, we reported taxa-specific neurotoxicity of denmotoxin from *Boiga dendrophila* (12) and irditoxin from *Boiga irregularis* (13). Taxa specificity manifests the natural targeting of the venom toxins toward their prey (13, 57–59). Snakes from the *Boiga* sp. mainly feed on the non-mammalian prey such as birds (12, 13, 60), whereas elapids, including the king cobra, mainly prey on snakes and rodents and only occasionally and opportunistically on birds (61, 62). Venom compositions of snakes are known to be dependent on prey specificity to ensure efficiency in their capture and killing (58). Therefore, the taxa-specific reversibility of the neuromuscular blockade produced by haditoxin is likely due to the natural species specificity of the king cobra venom and not because of low toxicity.

Structurally Important Residues for Haditoxin—Haditoxin contains all 8 conserved cysteine residues that are essential for the three-finger folding (24, 63). They form four disulfide bridges located in the core region of the molecule. In addition, this molecule possesses several other structurally invariant residues, responsible for the stability of the three-finger fold. For example, Tyr-25 (numbering of the residues is according to erabutoxin-a, unless stated otherwise), the crucial residue stabilizing the antiparallel β-sheet structure (64), is conserved in a similar three-dimensional orientation. Similarly, the structurally invariant Gly-40, involved in the tight packing of the three-dimensional fold by accommodating the bulky side chain of the Tyr-25 (24), is also conserved. The 2 proline residues Pro-44 and Pro-48, potentially associated with the formation of the β-turn (24), are conserved in haditoxin as Pro-46 and Pro-50. The salt bridge between the

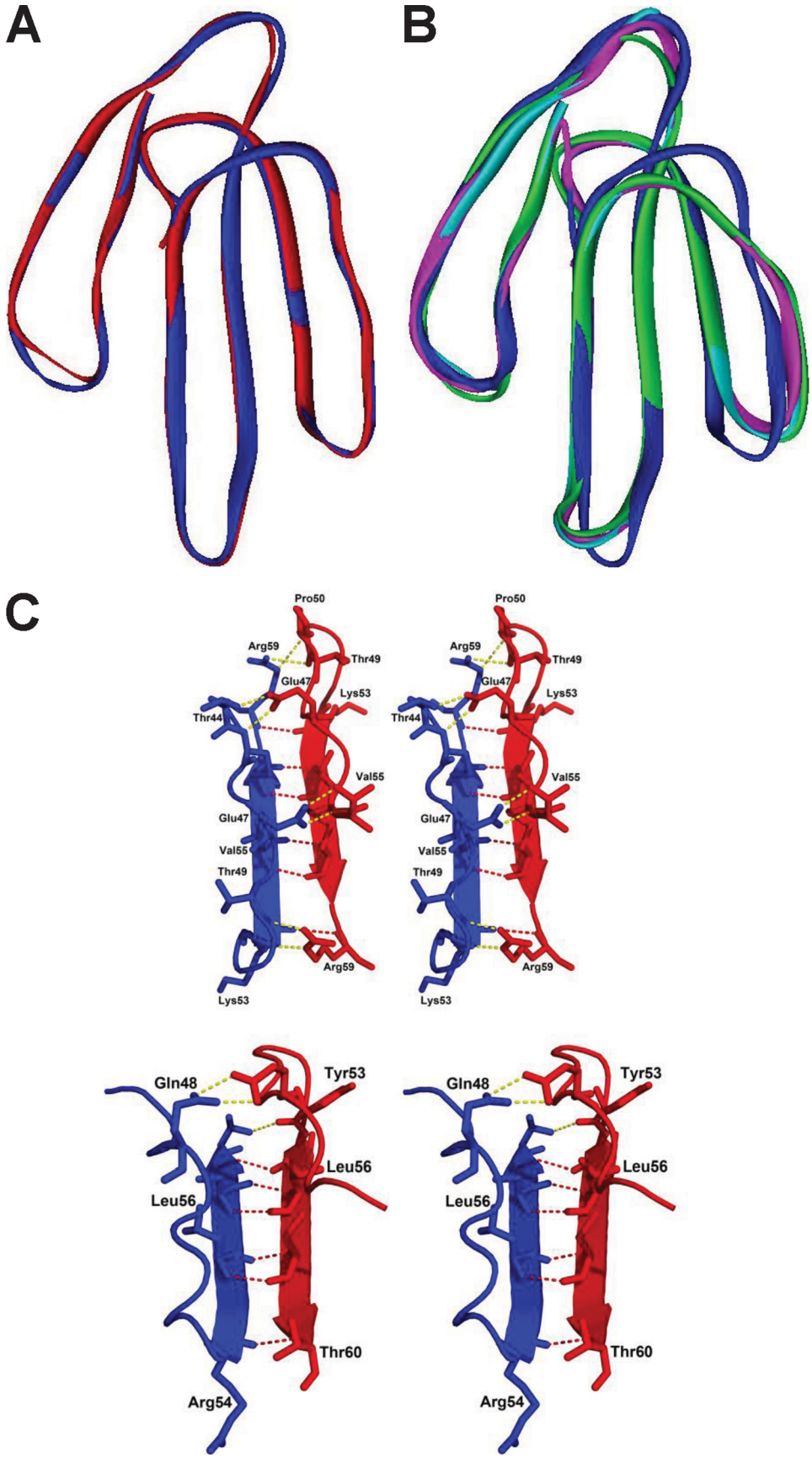

TABLE 2
Hydrogen bonds in the dimeric interface of the haditoxin

Hydrogen bonds	Monomer A	Monomer B	Distance
			Å
Main chain-main chain	Cys-57 (O)	Val-55 (N)	2.93
	Val-55 (O)	Cys-57 (N)	2.85
	Cys-57 (N)	Val-55 (O)	2.86
	Val-55 (N)	Cys-57 (O)	2.90
	Lys-53 (O)	Arg-59 (N)	3.10
	Arg-59 (N)	Lys-53 (O)	3.40
Side chain-side chain	Glu-47 (OE1)	Thr-44 (OG1)	2.63
	Glu-47 (OE2)	Cys-45 (N)	2.76
	Pro-50 (O)	Arg-59 (NE)	3.39
	Thr-49 (O)	Arg-59 (NH_2)	3.37
	Thr-44 (OG1)	Glu-47 (OE1)	2.68
	Cys-45 (N)	Glu-47 (OE2)	2.81
	Arg-59 (NH_2)	Thr-49 (O)	2.66
	Arg-59 (NE)	Gly-52 (O)	2.76

N-terminal amino group and the carboxyl group of Glu-58 as well as the C-terminal carboxyl group and the guanidinium group of Arg-39 in erabutoxin-a (24) is maintained by the N-terminal amino group and the carboxyl group of Asp-58 as well as the C-terminal carboxyl group and the guanidinium group of the Arg-39 in haditoxin. Thus, the presence of these structurally invariant residues contributes to the stable three-finger fold of haditoxin.

Functionally Important Residues for Haditoxin—Extensive structure-function relationship studies on the short-chain α-neurotoxin, erabutoxin-a (24, 65, 66), and the long-chain α-neurotoxins, α-cobratoxin (67, 68) and α-bungarotoxin (69, 70), revealed the critical residues involved in the recognition of nAChRs by snake neurotoxins. The crucial residues for α-neurotoxins to bind to muscle (αβγδ) nAChRs are Lys-27, Trp-29, Asp-31, Phe-32, Arg-33, and Lys-47. Haditoxin possesses three of them (Trp-29, Asp-31, and Arg-33) in homologous positions. Additionally, each type of toxin possesses specific residues that recognize muscle or neuronal nAChRs. For muscle (αβγδ) nAChRs, these are His-6, Gln-7, Ser-8, Ser-9, and Gln-10 in loop I and Tyr-25, Gly-34, Ile-36, and Glu-38 in loop II of short-chain α-neurotoxins (65) and Arg-36 in loop II and Phe-65 in the C terminus tail of long-chain α-neurotoxins (67). His-6, Gln-7, and Ser-8 in the loop I and Tyr-25, Gly-34, Ile-37, and Glu-38 in the loop II are conserved in haditoxin as the muscle subtype-specific determinants of short-chain α-neurotoxins. Moreover, Arg-36, muscle subtype-specific determinant of long-chain α-neurotoxins, is also conserved in haditoxin. The presence of these multiple functional determinants may explain the potent neurotoxicity exhibited by haditoxin on mammalian and avian muscle (αβγδ) nAChR.

On the contrary, the specific determinants (Ala-28 and Lys-35; α-cobratoxin numbering) of long-chain α-neurotoxins toward the neuronal (α_7) nAChRs (71) are not conserved in haditoxin. Significantly, haditoxin also lacks the fifth disulfide bridge responsible for the cyclization of loop II, which is considered to be a hallmark determinant for the ability of neurotoxins such as α-bungarotoxin and κ-bungarotoxins to interact with their specific neuronal nAChR targets (67, 71–74). This is somewhat surprising given the high affinity of haditoxin for α_7- (IC_{50} = 0.18 μM), $\alpha_3\beta_2$- (IC_{50} = 0.5 μM), and $\alpha_4\beta_2$- (IC_{50} = 2.6 μM) nAChRs. Previously, candoxin, a non-conventional 3FTx (31), was found to be an exception of a 3FTx that did not have the fifth disulfide bridge in loop II (candoxin has a fifth disulfide bridge in loop I) but still retained the ability to interact with neuronal (α_7) nAChRs (75). It was suggested thus that candoxin may likely interact with neuronal α_7-nAChRs using alternate, novel points of contact. Likewise, it is plausible that haditoxin possesses unique combinations of determinants that enable its interaction with α_7-, as well as $\alpha_3\beta_2$- and $\alpha_4\beta_2$-nAChRs. A detailed structure-function analysis to decipher these novel determinants is beyond the scope of this report.

In the case of κ-neurotoxins, which interact with neuronal $\alpha_3\beta_2$- and $\alpha_4\beta_2$-nAChRs with high affinity (26, 27), the critical functional residue was identified as Arg-34 (76). Haditoxin has Arg-33 in a homologous position, which may contribute in part to high affinity interaction with $\alpha_3\beta_2$- (IC_{50} = 0.5 μM) and $\alpha_4\beta_2$- (IC_{50} = 2.6 μM) nAChRs. Mutagenesis studies on κ-bungarotoxin revealed that the replacement of Pro-36 to an amino acid residue bearing a bulky, charged side chain, such as the Lys found in α-bungarotoxin, causes a 16-fold decrease in the efficacy of the toxin to block neurotransmission in the chick ciliary ganglion assay (76). Haditoxin bears an equivalent glycine residue, lacking a bulky, charged side chain, which can explain the high affinity of this toxin toward the neuronal ($\alpha_3\beta_2$ and $\alpha_4\beta_2$) nAChRs.

Comparison of Haditoxin with Other Dimeric 3FTxs—Few known examples of dimeric three-finger neurotoxins derived from snake venoms exist (13, 37, 72). Among them, the most well studied and characterized are the κ-neurotoxins, known to be composed of two identical monomers held together by non-covalent interactions (77, 78). The observed dimeric form of haditoxin, with the characteristic six β-pleated sheets, is similar to that formed by κ-bungarotoxin (77). Superposition of both molecules yielded an r.m.s.d. of 1.95 Å for 104 Cα atoms (Fig. 8*A*). The major deviations are located in the loops between the antiparallel β-strands. However, each monomer in κ-bungarotoxin is structurally homologous to long-chain α-neurotoxins unlike haditoxin, which resembles short-chain α-neurotoxins (Fig. 7*C*). The dimeric interface for both is maintained by six main chain-main chain hydrogen bonds (77). In addition, haditoxin has eight side chain hydrogen-bonding contacts between the monomers, whereas only three similar contacts were observed in κ-bungarotoxin (Fig. 7*A*) (77), suggesting that haditoxin forms tighter dimers than κ-bungarotoxin. The side chain interactions in κ-bungarotoxin are maintained by Phe-49, Leu-57, and Ile-20, which are strictly conserved in all κ-neurotoxins (77, 79). Mutagenesis studies have proven that replacing Phe-49 or Ile-20 with alanines renders a toxin with an apparent lack of ability to fold into the native structure, even as a monomer (79).

FIGURE 7. **Structural details of haditoxin.** *A*, superimposition of both subunits of haditoxin. Subunits A and B are shown in *blue* and *red*, respectively. *B*, superimposition subunit A of haditoxin with short-chain α-neurotoxins. Subunit A is shown in *blue*, erabutoxin-a is shown in *magenta*, erabutoxin-b is shown in *cyan*, and toxin-α is shown in *green*. *C*, stereo diagram of comparison of dimer interface of haditoxin (*top*) and κ-bungarotoxin (*bottom*). The residues to form the hydrogen bonds are labeled. The main chain-main chain hydrogen bonds are shown in *red*, and the other hydrogen bonds are shown in *yellow*.

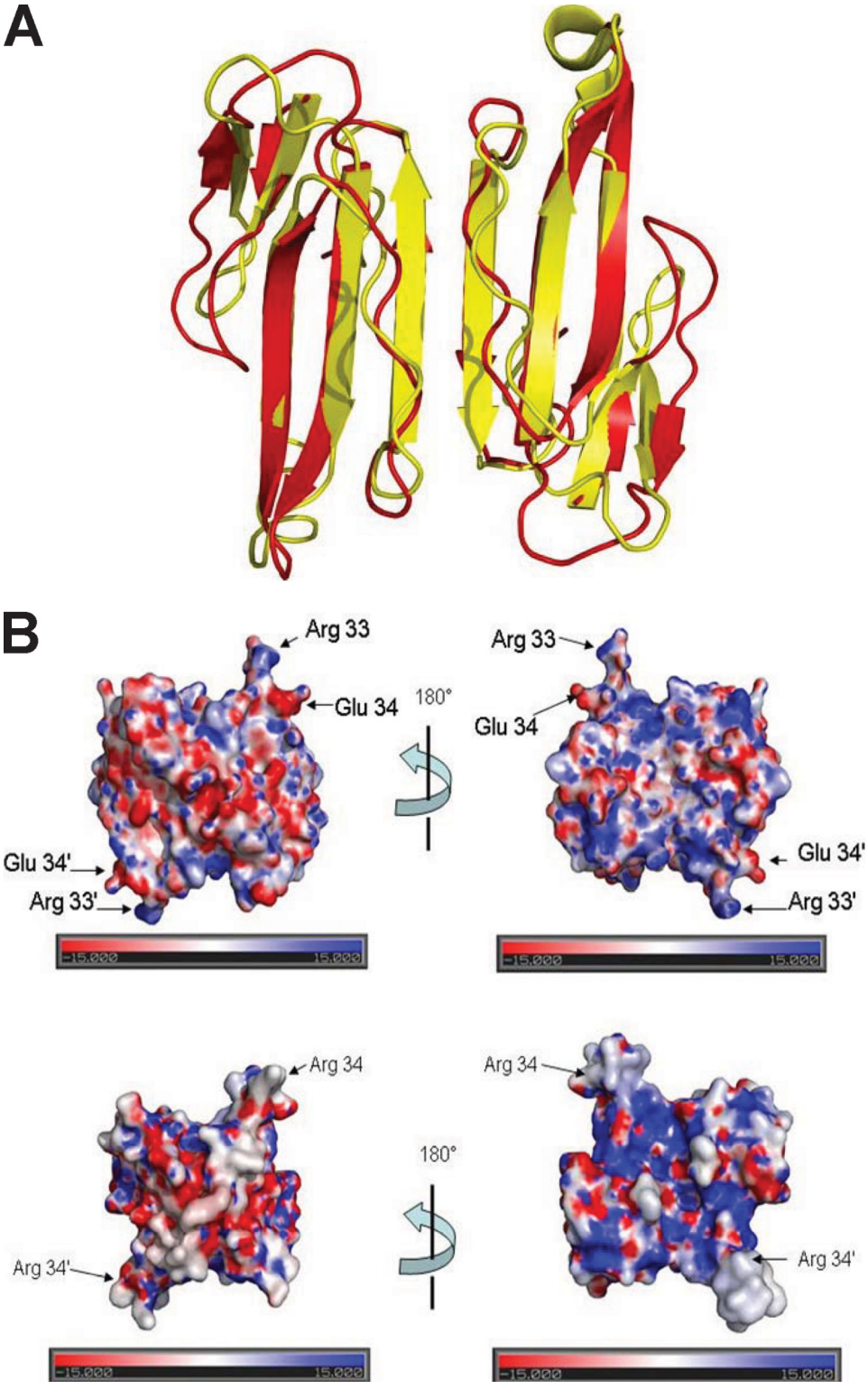

FIGURE 8. **Haditoxin *versus* κ-bungarotoxin.** *A*, superimposition of haditoxin with κ-bungarotoxin. Haditoxin and κ-bungarotoxin are shown in *red* and *yellow*, respectively. *B*, electrostatic surface of haditoxin (*top*) and κ-bungarotoxin (*bottom*). The orientation is the same as in Fig. 6*B*. The locations of Arg-33 and Glu-34 of haditoxin and Arg-34 of κ-bungarotoxin are indicated.

intact dimeric structure. The electrostatic surface potentials for both molecules were apparently similar (Fig. 8*B*) except for the tip of loop II, which revealed a strong positive patch for haditoxin when compared with κ-bungarotoxin (77).

Functionally, κ-neurotoxins interact with the neuronal ($\alpha_3\beta_2$ and $\alpha_4\beta_2$) nAChRs with high affinity (26, 27), whereas haditoxin interacts with both muscle ($\alpha\beta\gamma\delta$) and a variety of neuronal (α_7, $\alpha_3\beta_2$, and $\alpha_4\beta_2$) nAChRs. The crystal structure of the κ-bungarotoxin dimer showed that the guanidinium groups of the essential arginine residues, situated at the tip of the loop II, maintains nearly identical distance (44 Å) (77), like the acetylcholine binding sites in the pentameric receptor (30–50 Å) (80, 81). The κ-bungarotoxin dimer may both interact with the acetylcholine binding sites on a single neuronal receptor and physically block ion flow by spanning the channel (77, 79). However, this mode of interaction does not explain the inability of the κ-neurotoxins to block the muscle nAChRs. Haditoxin maintains a distance of ~52 Å between the guanidinium groups of the critical arginine residues present in the turn region of the second loop, which is almost similar to the acetylcholine binding sites in the pentameric receptor mentioned above. However, unlike the κ-neurotoxins, haditoxin interacts with both muscle and neuronal nAChRs. This supports the fact that the dimeric toxins may have a unique mode of interaction with the nAChRs, which demands further investigation.

More recently, other heterodimeric 3FTxs from elapid venoms have been reported, including covalently (disulfide) linked homodimers of a long-chain α-neurotoxin (α-cobratoxin) and heterodimers of α-cobratoxin in combination with a variety of three-finger cytotoxins (72). Unlike haditoxin, all of these dimers are formed by covalent bonding (disulfide linkage) of the monomeric units. Functionally, the α-cobratoxin-cytotoxin heterodimers were able to block neuronal (α_7) nAChRs, whereas the α-cobratoxin homodimer exhibited blockade of

The same result has been observed with deletion studies (deletion of Arg-54) with an aim to generate a 65-residue-long protein, as found in the α-neurotoxins, from the 66-residue-long κ-bungarotoxin (79), whereas haditoxin being a 65-residue-long protein lacks both Phe-49 and Ile-20 but still retains the

both neuronal α_7- and $\alpha_3\beta_2$-nAChRs, unlike monomeric α-cobratoxin, which interacts with muscle ($\alpha\beta\gamma\delta$) and neuronal (α_7) nAChRs (72).

Our laboratory has also reported on a colubrid venom-derived covalently linked heterodimeric 3FTx, irditoxin (13), which was found to target muscle ($\alpha\beta\gamma\delta$) nAChRs, in sharp contrast to the reported function of elapid dimeric toxins (72). Another distinguishing feature was that the subunits of irditoxin structurally resemble non-conventional 3FTxs (13). Haditoxin is both structurally and functionally distinct from the α-cobratoxin hetero/homodimers as well as irditoxin. Structurally, haditoxin is a non-covalently linked homodimer of the short-chain α-neurotoxin type, and functionally, it has a broad pharmacological profile with high affinity and selectivity for muscle ($\alpha\beta\gamma\delta$) and neuronal (α_7, $\alpha_4\beta_2$, and $\alpha_3\beta_2$) nAChRs. Haditoxin exhibits a unique structural and functional profile and is the first reported dimeric 3FTx interacting with the muscle ($\alpha\beta\gamma\delta$) nAChR as well as the first short-chain type of α-neurotoxin to interact with neuronal α_7-nAChR with nanomolar affinity.

REFERENCES

1. Harvey, A. L. (1991) *Snake Toxins*, pp. 1–90, Pergamon Press, New York
2. Lewis, R. J., and Garcia, M. L. (2003) *Nat. Rev. Drug Discov.* **2,** 790–802
3. Harvey, A. L. (2002) *Trends Pharmacol. Sci.* **23,** 201–203
4. Langley, J. N. (1907) *J. Physiol.* **36,** 347–384
5. Katz, B., and Thesleff, S. (1957) *J. Physiol.* **138,** 63–80
6. Grutter, T., and Changeux, J. P. (2001) *Trends Biochem. Sci.* **26,** 459–463
7. Changeux, J. P. (1990) *Trends Pharmacol. Sci.* **11,** 485–492
8. Taylor, P., Molles, B., Malany, S., and Osaka, H. (2002) in *Perspectives in Molecular Toxinology* (Ménez, A., ed) pp. 271–280, John Wiley & Sons, Chichester, England
9. Changeux, J. P., Kasai, M., and Lee, C. Y. (1970) *Proc. Natl. Acad. Sci. U.S.A.* **67,** 1241–1247
10. Colquhoun, L. M., and Patrick, J. W. (1997) *Adv. Pharmacol.* **39,** 191–220
11. Kini, R. M. (2002) *Clin. Exp. Pharmacol. Physiol.* **29,** 815–822
12. Pawlak, J., Mackessy, S. P., Fry, B. G., Bhatia, M., Mourier, G., Fruchart-Gaillard, C., Servent, D., Ménez, R., Stura, E., Ménez, A., and Kini, R. M. (2006) *J. Biol. Chem.* **281,** 29030–29041
13. Pawlak, J., Mackessy, S. P., Sixberry, N. M., Stura, E. A., Le Du, M. H., Ménez, R., Foo, C. S., Ménez, A., Nirthanan, S., and Kini, R. M. (2009) *FASEB J.* **23,** 534–545
14. Pahari, S., Mackessy, S. P., and Kini, R. M. (2007) *BMC. Mol. Biol.* **8,** 115
15. Jiang, M., Häggblad, J., and Heilbronn, E. (1987) *Toxicon* **25,** 1019–1022
16. Tsetlin, V. (1999) *Eur. J. Biochem.* **264,** 281–286
17. Kumar, T. K., Jayaraman, G., Lee, C. S., Arunkumar, A. I., Sivaraman, T., Samuel, D., and Yu, C. (1997) *J. Biomol. Struct. Dyn.* **15,** 431–463
18. de Weille, J. R., Schweitz, H., Maes, P., Tartar, A., and Lazdunski, M. (1991) *Proc. Natl. Acad. Sci. U.S.A.* **88,** 2437–2440
19. McDowell, R. S., Dennis, M. S., Louie, A., Shuster, M., Mulkerrin, M. G., and Lazarus, R. A. (1992) *Biochemistry* **31,** 4766–4772
20. Rajagopalan, N., Pung, Y. F., Zhu, Y. Z., Wong, P. T., Kumar, P. P., and Kini, R. M. (2007) *FASEB J.* **21,** 3685–3695
21. Ricciardi, A., le Du, M. H., Khayati, M., Dajas, F., Boulain, J. C., Menez, A., and Ducancel, F. (2000) *J. Biol. Chem.* **275,** 18302–18310
22. Ohno, M., Ménez, R., Ogawa, T., Danse, J. M., Shimohigashi, Y., Fromen, C., Ducancel, F., Zinn-Justin, S., Le Du, M. H., Boulain, J. C., Tamiya, T., and Ménez, A. (1998) *Prog. Nucleic Acid Res. Mol. Biol.* **59,** 307–364
23. Nirthanan, S., and Gwee, M. C. (2004) *J. Pharmacol. Sci.* **94,** 1–17
24. Endo, T., and Tamiya, N. (1991) in *Snake Toxins* (Harvey, A. L., ed) pp. 165–222, Pergamon Press, New York
25. Servent, D., Antil-Delbeke, S., Gaillard, C., Corringer, P. J., Changeux, J. P., and Ménez, A. (2000) *Eur. J. Pharmacol.* **393,** 197–204
26. Grant, G. A., and Chiappinelli, V. A. (1985) *Biochemistry* **24,** 1532–1537
27. Wolf, K. M., Ciarleglio, A., and Chiappinelli, V. A. (1988) *Brain Res.* **439,** 249–258
28. Servent, D., and Fruchart-Gaillard, C. (2009) *J. Neurochem.* **109,** 1193–1202
29. Harvey, A. L., Kornisiuk, E., Bradley, K. N., Cerveñansky, C., Durán, R., Adrover, M., Sánchez, G., and Jerusalinsky, D. (2002) *Neurochem. Res.* **27,** 1543–1554
30. Olianas, M. C., Ingianni, A., Maullu, C., Adem, A., Karlsson, E., and Onali, P. (1999) *J. Pharmacol. Exp. Ther.* **288,** 164–170
31. Nirthanan, S., Charpantier, E., Gopalakrishnakone, P., Gwee, M. C., Khoo, H. E., Cheah, L. S., Bertrand, D., and Kini, R. M. (2002) *J. Biol. Chem.* **277,** 17811–17820
32. Lumsden, N. G., Fry, B. G., Ventura, S., Kini, R. M., and Hodgson, W. C. (2005) *Toxicon* **45,** 329–334
33. Starkov, V. G., Poliak, Iu. L., Vul'fius, E. A., Kriukova, E. V., Tsetlin, V. I., and Utkin, Iu. N. (2009) *Bioorg. Khim.* **35,** 15–24
34. Kuruppu, S., Reeve, S., Smith, A. I., and Hodgson, W. C. (2005) *Biochem. Pharmacol.* **70,** 794–800
35. Tan, L. C., Kuruppu, S., Smith, A. I., Reeve, S., and Hodgson, W. C. (2006) *Neuropharmacology* **51,** 782–788
36. Aird, S. D., Womble, G. C., Yates, J. R., 3rd, and Griffin, P. R. (1999) *Toxicon* **37,** 609–625
37. Chiappinelli, V. A., and Lee, J. C. (1985) *J. Biol. Chem.* **260,** 6182–6186
38. Chiappinelli, V. A., and Wolf, K. M. (1989) *Biochemistry* **28,** 8543–8547
39. Ginsborg, B. L., and Warriner, J. (1960) *Br. J. Pharmacol. Chemother.* **15,** 410–411
40. Bülbring, E. (1997) *Br. J. Pharmacol.* **120,** 3–26
41. Hogg, R. C., Bandelier, F., Benoit, A., Dosch, R., and Bertrand, D. (2008) *J. Neurosci. Methods* **169,** 65–75
42. Staros, J. V. (1982) *Biochemistry* **21,** 3950–3955
43. Otwinowski, Z., and Minor, W. (1997) *Methods Enzymol.* **276,** 307–326
44. Pung, Y. F., Wong, P. T., Kumar, P. P., Hodgson, W. C., and Kini, R. M. (2005) *J. Biol. Chem.* **280,** 13137–13147
45. Coulson, F. R., Jacoby, D. B., and Fryer, A. D. (2004) *J. Pharmacol. Exp. Ther.* **308,** 760–766
46. Weiser, M., Mutschler, E., and Lambrecht, G. (1997) *Naunyn Schmiedebergs Arch. Pharmacol.* **356,** 671–677
47. Warrell, D. A., Looareesuwan, S., White, N. J., Theakston, R. D., Warrell, M. J., Kosakarn, W., and Reid, H. A. (1983) *Br. Med. J.* (*Clin. Res. Ed.*) **286,** 678–680
48. Laothong, C., and Sitprija, V. (2001) *Toxicon* **39,** 1353–1357
49. Palma, E., Bertrand, S., Binzoni, T., and Bertrand, D. (1996) *J. Physiol.* **491,** 151–161
50. Vagin, A., and Teplyakov, A. (1997) *J. Appl. Crystallogr.* **30,** 1022–1025
51. Vagin, A. A., Steiner, R. A., Lebedev, A. A., Potterton, L., McNicholas, S., Long, F., and Murshudov, G. N. (2004) *Acta Crystallogr. D. Biol. Crystallogr.* **60,** 2184–2195
52. Perrakis, A., Morris, R., and Lamzin, V. S. (1999) *Nat. Struct. Biol.* **6,** 458–463
53. Emsley, P., and Cowtan, K. (2004) *Acta Crystallogr. D. Biol. Crystallogr.* **60,** 2126–2132
54. Laskowski, R. A., MacArthur, M. W., Moss, D. S., and Thornton, J. M. (1993) *J. Appl. Crystallogr.* **26,** 283–291
55. Berman, H. M., Westbrook, J., Feng, Z., Gilliland, G., Bhat, T. N., Weissig, H., Shindyalov, I. N., and Bourne, P. E. (2000) *Nucleic Acids Res.* **28,** 235–242
56. Krissinel, E., and Henrick, K. (2007) *J. Mol. Biol.* **372,** 774–797
57. Barlow, A., Pook, C. E., Harrison, R. A., and Wüster, W. (2009) *Proc. Biol. Sci.* **276,** 2443–2449
58. Daltry, J. C., Wüster, W., and Thorpe, R. S. (1996) *Nature* **379,** 537–540
59. Pahari, S., Bickford, D., Fry, B. G., and Kini, R. M. (2007) *BMC. Evol. Biol.* **7,** 175
60. Mackessy, S. P., Sixberry, N. M., Heyborne, W. H., and Fritts, T. (2006) *Toxicon* **47,** 537–548
61. Mehrtens, J. (1987) *Living Snakes of the World*, pp. 245–281, Sterling, New York
62. Coborn, J. (1991) *The Atlas of Snakes of the World*, pp. 452–453, TFH Publications, New Jersey

63. Ménez, A., Bouet, F., Guschlbauer, W., and Fromageot, P. (1980) *Biochemistry* **19,** 4166–4172
64. Torres, A. M., Kini, R. M., Selvanayagam, N., and Kuchel, P. W. (2001) *Biochem. J.* **360,** 539–548
65. Teixeira-Clerc, F., Ménez, A., and Kessler, P. (2002) *J. Biol. Chem.* **277,** 25741–25747
66. Trémeau, O., Lemaire, C., Drevet, P., Pinkasfeld, S., Ducancel, F., Boulain, J. C., and Ménez, A. (1995) *J. Biol. Chem.* **270,** 9362–9369
67. Bourne, Y., Talley, T. T., Hansen, S. B., Taylor, P., and Marchot, P. (2005) *EMBO J.* **24,** 1512–1522
68. Antil, S., Servent, D., and Ménez, A. (1999) *J. Biol. Chem.* **274,** 34851–34858
69. Fruchart-Gaillard, C., Gilquin, B., Antil-Delbeke, S., Le Novère, N., Tamiya, T., Corringer, P. J., Changeux, J. P., Ménez, A., and Servent, D. (2002) *Proc. Natl. Acad. Sci. U.S.A.* **99,** 3216–3221
70. Dellisanti, C. D., Yao, Y., Stroud, J. C., Wang, Z. Z., and Chen, L. (2007) *Nat. Neurosci.* **10,** 953–962
71. Antil-Delbeke, S., Gaillard, C., Tamiya, T., Corringer, P. J., Changeux, J. P., Servent, D., and Ménez, A. (2000) *J. Biol. Chem.* **275,** 29594–29601
72. Osipov, A. V., Kasheverov, I. E., Makarova, Y. V., Starkov, V. G., Vorontsova, O. V., Ziganshin, R. Kh., Andreeva, T. V., Serebryakova, M. V., Benoit, A., Hogg, R. C., Bertrand, D., Tsetlin, V. I., and Utkin, Y. N. (2008) *J. Biol. Chem.* **283,** 14571–14580
73. Grant, G. A., Luetje, C. W., Summers, R., and Xu, X. L. (1998) *Biochemistry* **37,** 12166–12171
74. Servent, D., Mourier, G., Antil, S., and Ménez, A. (1998) *Toxicol. Lett.* **102–103,** 199–203
75. Nirthanan, S., Charpantier, E., Gopalakrishnakone, P., Gwee, M. C., Khoo, H. E., Cheah, L. S., Kini, R. M., and Bertrand, D. (2003) *Br. J. Pharmacol.* **139,** 832–844
76. Fiordalisi, J. J., al-Rabiee, R., Chiappinelli, V. A., and Grant, G. A. (1994) *Biochemistry* **33,** 3872–3877
77. Dewan, J. C., Grant, G. A., and Sacchettini, J. C. (1994) *Biochemistry* **33,** 13147–13154
78. Oswald, R. E., Sutcliffe, M. J., Bamberger, M., Loring, R. H., Braswell, E., and Dobson, C. M. (1991) *Biochemistry* **30,** 4901–4909
79. Grant, G. A., Al-Rabiee, R., Xu, X. L., and Zhang, Y. (1997) *Biochemistry* **36,** 3353–3358
80. Herz, J. M., Johnson, D. A., and Taylor, P. (1989) *J. Biol. Chem.* **264,** 12439–12448
81. Unwin, N. (1993) *J. Mol. Biol.* **229,** 1101–1124
82. Gille, C., and Frömmel, C. (2001) *Bioinformatics* **17,** 377–378
83. Gouet, P., Courcelle, E., Stuart, D. I., and Métoz, F. (1999) *Bioinformatics* **15,** 305–308